NJC

New Journal of Chemistry

A journal for new directions in chemistry

Accepted Manuscript

This article can be cited before page numbers have been issued, to do this please use: S. Li, W. Xia, Y. Zhang and Z. Tao, *New J. Chem.*, 2020, DOI: 10.1039/D0NJ01755H.

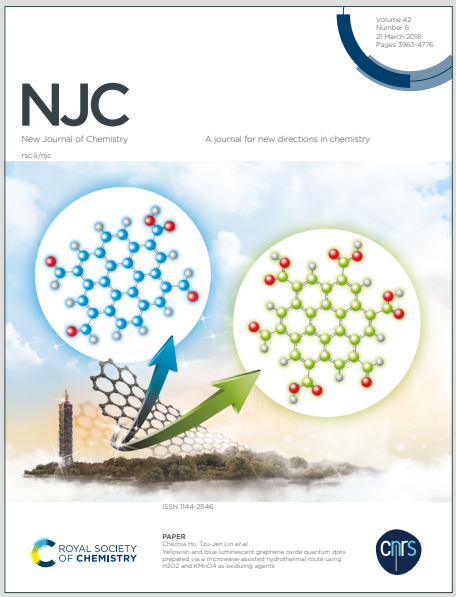

This is an Accepted Manuscript, which has been through the Royal Society of Chemistry peer review process and has been accepted for publication.

Accepted Manuscripts are published online shortly after acceptance, before technical editing, formatting and proof reading. Using this free service, authors can make their results available to the community, in citable form, before we publish the edited article. We will replace this Accepted Manuscript with the edited and formatted Advance Article as soon as it is available.

You can find more information about Accepted Manuscripts in the Information for Authors.

Please note that technical editing may introduce minor changes to the text and/or graphics, which may alter content. The journal's standard Terms & Conditions and the Ethical guidelines still apply. In no event shall the Royal Society of Chemistry be held responsible for any errors or omissions in this Accepted Manuscript or any consequences arising from the use of any information it contains.

Self-Assembled Tetramethylcucurbit[6]uril-Polyoxometalate Nanocubes as Efficient and Recyclable Catalysts for Preparation of Propyl gallate

Shuang Li, Wen Xia, Yunqian Zhang*, Zhu Tao

Key Laboratory of Macrocyclic and Supramolecular Chemistry of Guizhou Province,

Guizhou University,

Guiyang 550025, China

*Corresponding to: sci.yqzhang@gzu.edu.cn (Y. Q. Zhang)

Abstract: The development of cucurbit[*n*]urils-polyoxometalates (Q[*n*]-POMs) hybrids with the same microshape and nanoscale features is highly desirable, *yet* remains a great challenge. Herein, we design and synthesize a class of Q[*n*]-POMs hybrids, tetramethyl cucurbit[6]uril-phosphomolybdic acid (TMeQ[6]-PMA) nanocubes (NCs), *via* an facile one-step self-assembly method, as heterogeneous acid catalysts for greatly boosting catalyst in term of activity and stability for the esterification of gallic acid and n-propanol to propyl gallate (PG). The fourier transform infrared (FTIR) spectroscopy reveals that the self-assembled mechanism of TMeQ[6]-PMA NCs based on the outer-surface interaction of Q[*n*]s. The temperature programmed desorption experiments with ammonia and FTIR analysis of pre-adsorbed pyridine results confirm that the coexistence of medium and strong acid sites and a larger number of Lewis acid sites than the Brönsted acidic sites on the catalyst surface. These new features make as-prepared TMeQ[6]-PMA NCs exhibit a high PG conversion (95.6 %) and excellent stability, which represents the best catalytic performances than other reported catalysts.

Keywords: tetramethyl cucurbit[6]uril; polyoxometalates; catalyst; propyl gallate

1. Introduction

Over the past few decades, catalysts, acid catalysts in particular, which can be divided into homogeneous as well as heterogeneous, play an important role in petrochemical, fine chemical and environmental industries.[1-5] Among them, the homogeneous acid catalysts such as sulfuric acid, phosphoric acid, hydrochloric acid, hydrofluoric acid as well as *p*-toluene sulfonic acid and so on, have been extensively applied in acid-catalyzed reactions.[6-10] Nevertheless, owing to their lethal drawbacks including corrosive nature, difficulty of separation and recovery, high pollution, high energy consumption and low water tolerance,[2, 9] seeking heterogeneous acid catalysts with high catalytic activity, no contamination, easy separation, as well as excellent stability is urgently desirable.

Recently, polyoxometalates (POMs), an exciting type of subnanometer-sized transition metal-oxygen clusters, have attracted extensive research interest as heterogeneous acid catalysts owing to their strong electron-accepting ability.[11-16] However, the major disadvantages of pristine POMs are low surface area hindering the exposure of active sites, and the difficulty of separation due to high solubility in most of polar solvents,[12, 15] which inevitably restrict their practical applications in catalytic reactions. Immobilizing POMs on suitable supports[16-21] and constructing organic-POMs hybrids[22-25] have been regarded as two effective strategies to overcome above problem, and the latter is more promising than the former.

Cucurbit[*n*]urils (Q[*n*]s), as an emerging class of cage-like supramolecular organic compounds after cyclodetrin, calixarene, and crown ether, possess a rigid hydrophobic cavity, two identical carbonyl-laced portals and positive electrostatic potential outer surface.[26-29] They can act as ideal hosts as well as ligands to derived various Q[*n*]-based hybrids, which, therefore, has sparked enormous research attention recently, especially in POMs as guests.[30-37] For instance, Fang *et al*. first demonstrated that Q[6] and Q[8] as host can assemble with guest POMs through interaction of outer surface and thus greatly expand the application of the hybrids.[32] Simultaneously, Cao et al. successfully synthesized Q[6]-POMs hybrids *via* hydrogen bonding that possessed outstanding photocatalytic

activity and stability for the degradation of methyl orange.[33] Furthermore, two isostructural decamethyl Q[5]-POMs composites were prepared and displayed reversible photochromic property and photocatalytic activity.[34] Very recently, we also revealed that perhydroxylated Q[6] could coordinate with POMs through supramolecular interactions, thereby leading to formation of new supramolecular assemblies.[35] Inspired by the above cases, novel Q[*n*]-POMs hybrids with the same microshape and nanoscale features for catalytic reaction is promising, but it has not been explored thus far, to the best of our knowledge.

Herein, we report an extremely facile strategy to synthesize a new Q[*n*]-POMs hybrids with the same microshape and nanoscale features, tetramethyl cucurbit[6]uril-phosphomolybdic acid (TMeQ[6]-PMA) nanocubes (NCs) (**Scheme 1**), by one-step self-assembly method. The field-emission scanning electron microscopy (FESEM), transmission electron microscopy (TEM) and energy dispersive X-ray spectroscopy (EDX) results confirm that as-prepared TMeQ[6]-PMA NCs possess a microshape and nanoscale features, and the homogeneous dispersion of PMA on the hybrid. The fourier transform infrared (FTIR) spectroscopy reveals that the self-assembled mechanism of TMeQ[6]-PMA NCs based on outer-surface interactions. The temperature programmed desorption experiments with ammonia (NH_3-TPD-MS) and FTIR analysis of pre-adsorbed pyridine (py-FTIR) on catalyst under vacuum at different temperatures demonstrate that the coexistence of medium and strong acid sites and a larger number of Lewis acid sites than the Brönsted acidic sites on the catalyst surface. To evaluate the catalytic activity of as-prepared TMeQ[6]-PMA NCs, the synthesis of propyl gallate (PG) which is widely applied in food antioxidant, cosmetics, adhesives, and lubricants industry,[38-40] was carried out. As a result, the as-prepared TMeQ[6]-PMA NCs exhibit a high PG conversion (95.6 %) and excellent stability, which represents the best catalytic performances than other reported catalysts.

View Article Online
DOI: 10.1039/D0NJ01755H

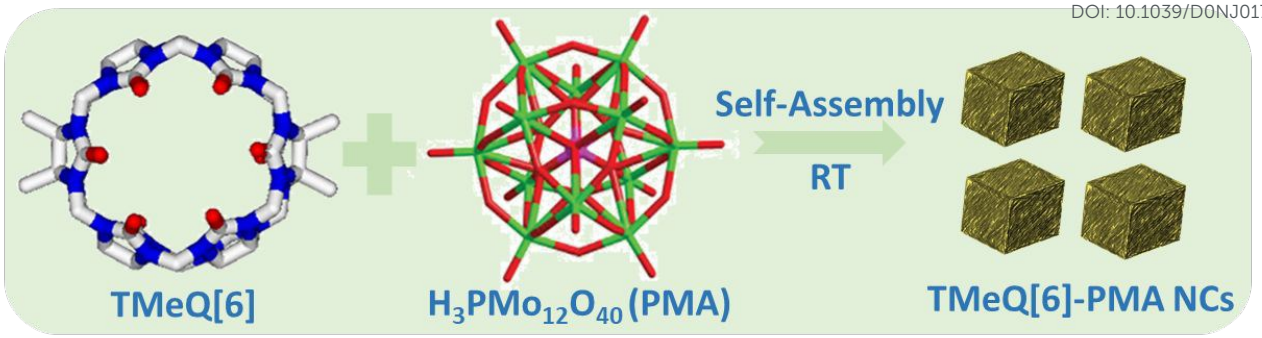

Scheme 1. Preparative route for TMeQ[6]-PMA NCs.

2. Results and discussions

2.1. *Morphological and structural characterization*

TMeQ[6]-PMA NCs were synthesized through a simple one-step self-assembly process. The morphology and elemental distribution of as-synthesized TMeQ[6]-PMA NCs, are investigated by FESEM, TEM as well as EDX, as shown in **Figure 1**. The low-magnification SEM image displays that the TMeQ[6]-PMA NCs are uniform, with a particle size of ~200 nm (**Figure 1 a**). The enlarged SEM image reveals that the surface of the composites is very rough, which is beneficial to the enhanced contact area between the catalyst and reactant, as shown in **Figure 1 b**. Moerover, the TEM image reveals that the TMeQ[6]-PMA nanocubes possess a particle size of ~200 nm which is in good agreement with SEM results (**Figure 1 c**). **Figure 1d** presents a typical TMeQ[6]-PMA NCs and the corresponding elemental mapping based on EDX is shown in **Figure 1e-i**. The C, N, O, Mo, and P elements are uniformly distributed on TMeQ[6]-PMA samples, suggesting the successful decoration of PMA into the composites. To confirm the chemical formula of as-prepared TMeQ[6]-PMA NCs, the elemental analysis was carried out (**Table S1**). The result indicates that chemical formula of as-prepared TMeQ[6]-PMA NCs is $C_{80}H_{97}N_{48}O_{144}P_3Mo_{36}{\cdot}nH_2O$.

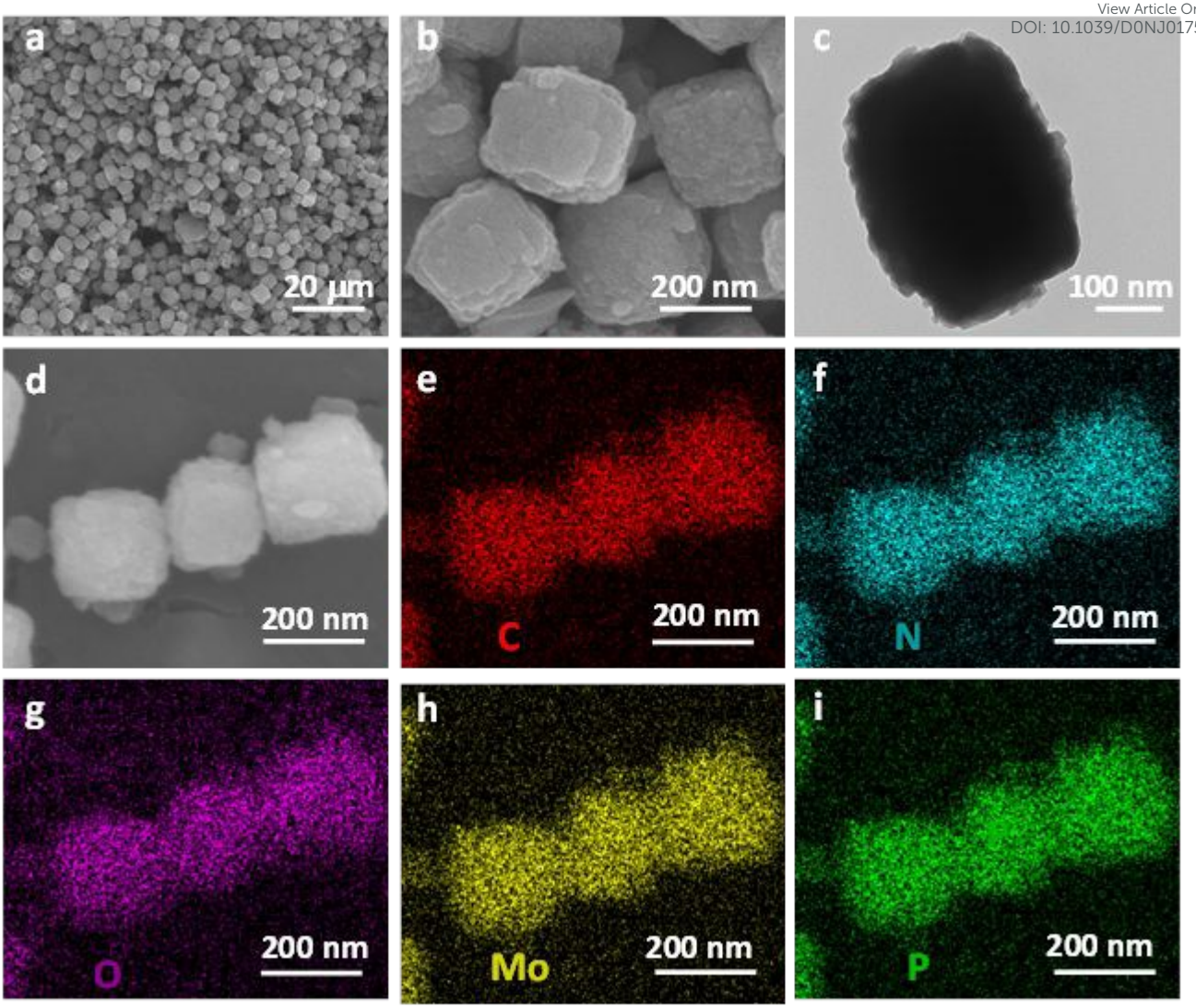

Figure 1. a, b) FESEM images and c) TEM image of the as-synthesized TMeQ[6]-PMA NCs. d) Typical SEM image of TMeQ[6]-PMA NCs and corresponding elemental mapping of e) C, f) N, g) O, h) Mo, and i) P elements.

The crystal structures of TMeQ[6], PMA, and as-prepared TMeQ[6]-PMA NCs are characterized by the powdered X-ray diffraction (PXRD) (**Figure 2a**). The results indicate that the both TMeQ[6] and PMA have obvious crystal characteristic peak. Furthermore, in the XRD pattern of the TMeQ[6]-PMA NCs, it is easy to observe the characteristic peaks of TMeQ[6], indicating that the introduction of PMA does not affect the crystal structure of TMeQ[6]. However, no evident peaks for PMA crystalline phases are discovered from XRD patterns of TMeQ[6]-PMA NCs, suggesting PMA clusters are successfully dispersed in the TMeQ[6] framework rather than existing as free solid acid. To further

confirm the self-assembled mechanism of composites, FTIR spectroscopy of pure TMeQ[6], PMA, as well as TMeQ[6]-PMA NCs in the range of 400-4000 cm^{-1} are characterized (**Figure 2b**). In the FTIR spectrum of the pure TMeQ[6], there are four distinct characteristic peaks at 2995-2930 cm^{-1} region (-CH_2), *ca.* 1747 (-C=O), and 1469 cm^{-1} (-CH_2). For the pure PMA with type Keggin structure displays several typical characteristic peaks at *ca.* 1065, 967, 871, and 790 cm^{-1}, which are attributes to the symmetric stretching vibrations of ν(P-O_a) in the central PO_4 tetrahedron, ν(Mo-O_d) in the exterior MoO_6 octahedron, ν(Mo-O_b-Mo) in the corner shared octahedron and ν(Mo-O_c-Mo) in the edge shared octahedron, respectively, in accordance with previous reports.[20] Moreover, the above characteristic peaks correspond to PMA could still be observed in the TMeQ[6]-PMA sample, suggesting that the initial Keggin structures of PMA preserve intact after the formation of the composites. In comparison with the FTIR spectrum of pure TMeQ[6], the peaks assigned to the bridged -CH_2 in the TMeQ[6]-PMA NCs have a red-shift of *ca.* 9 and 6 cm^{-1}, respectively, which is the result of the strong electrostatic interactions and formation of hydrogen bonds between TMeQ[6] and $[PMAO_{40}]^{3-}$. The thermogravimetry and differential scanning calorimetry (TG-DSC) were employed to investigate the thermal stability of TMeQ[6]-PMA NCs (**Figure 2c**). The result reveals impressive thermal stability, with a decomposition temperature up to 630 ^oC in N_2. Furthermore, the weight losses from 30 to 240 ^oC could be attributed to the removal of water molecules absorbed in the surface of TMeQ[6]-PMA NCs. From the nitrogen adsorption and desorption measurement (**Figure 2d**), the TMeQ[6]-PMA NCs shows mixed adsorption isotherms of type I and II adsorption-desorption isotherms.[41] The specific surface areas (SSA) and pore size distribution of TMeQ[6]-PMA NCs are characterized by the Brunauer-Emmett-Teller (BET) analysis and nonlocal density functional theory (NL-DFT), respectively. TMeQ[6]-PMA NCs possess a large SSA of 49.76 $m^3\ g^{-1}$ and a high pore volume of 0.055 $cm^3\ g^{-1}$ with a micropore diameter of around 0.95 nm.

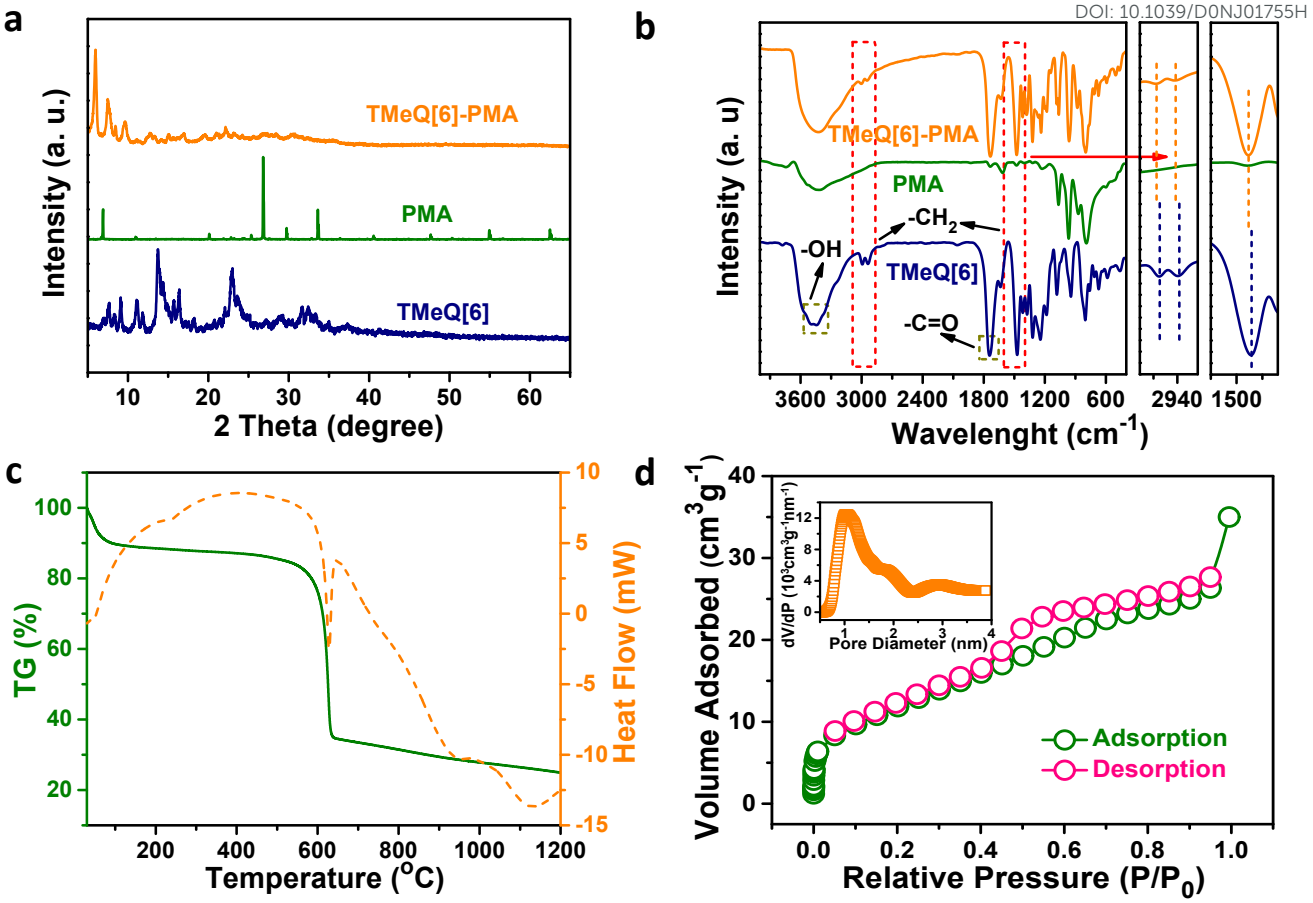

Figure 2. a) PXRD and b) FTIR patterns of TMeQ[6], PMA, and TMeQ[6]-PMA NCs. c) TG-DSC curves of TMeQ[6]-PMA NCs in N_2 at a heating rate of 10 ^oC min^{-1}. d) Nitrogen adsorption-desorption isotherms and pore size distribution (the inset) of TMeQ[6]-PMA NCs.

2.2. Surface acidic property

Surface acid property, including acid site, intensity and density, is a significant parameter, closely linked with the catalyst activity, which could be evaluated by NH_3-TPD-MS. The desorption temperature profiles and the amounts of desorption ammonia of the TMeQ[6]-PMA catalysts from 323 to 973 K are displayed in the **Figure 3a** and Figure S1, where three temperature zones correlated to the acid sites intensity (weak, medium and strong) can be differentiated according to the previous literature.[42,43] The result depicts that the TMeQ[6]-PMA NCs has three obvious desorption peaks at temperature of 633.5, 662.3, and 853.5 K with ammonia adsorption capacity was 11.3, 3.7 as well as 5.9 mmol g^{-1}, respectively (whereas the total number of acid sites was 20.9 mmol g^{-1}), which reveals

the co-presence of medium and strong acid sites on the catalyst surface. Moreover, the Brönsted acid sites and Lewis acid sites of as-prepared materials were further investigated by FTIR analysis of pre-adsorbed pyridine on catalyst under vacuum at different temperatures within the frequency range 1700-1400 cm^{-1} (**Figure 3b**). The spectrum of TMeQ[6]-PMA sample at 298 K displays five bands: band at 1447, 1576, and 1606 cm^{-1} correspond to the characteristic of pyridine adsorbed at Lewis acidic sites; bands at 1642 cm^{-1} is generally assigned to the coordinated pyridine bound to Brönsted acidic sites (PyH^+); the another band appeared at 1490 cm^{-1} reflects a both Brönsted acidic and Lewis acidic site toward pyridine adsorption.[44,45] As a result, the TMeQ[6]-PMA NCs exhibit a larger number of Lewis acid sites than the Brönsted acidic sites, and the frequencies for pyridine at Lewis acid sites are appeared at all temperatures, only changing in relative intensity between the bands, which indicate pyridine is not desorbed even at high temperatures.

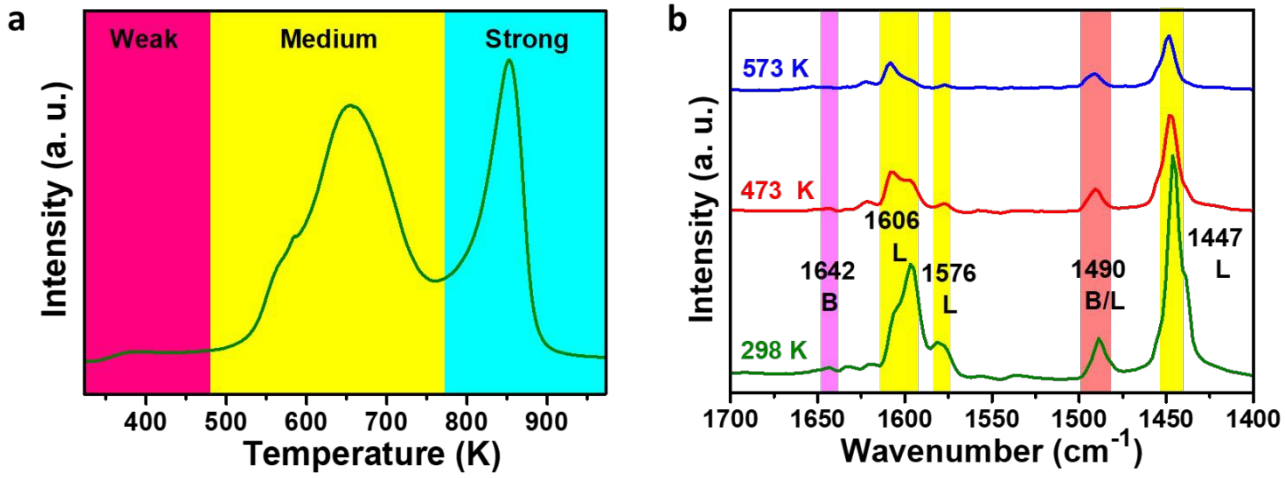

Figure 3. a) Temperature programmed desorption experiments with ammonia of TMeQ[6]-PMA NCs. b) FTIR analysis of pre-adsorbed pyridine on catalyst under vacuum at different temperatures of TMeQ[6]-PMA NCs.

2.3. Catalytic performance

Catalytic activity of the as-prepared TMeQ[6]-PMA catalysts were investigated in the esterification of gallic acid and n-propanol to propyl gallate, which is an important gallic acid ester with an excellent antioxidation capacity.[38-40] As illustrated in **Figure 4a**, the influence of reaction time

on conversion of PG was examined. The result suggests that the yield of PG underwent a dramatic rise at the initial stage followed by a slow decrease with the increase of reaction time. The maximum conversion (91.2 %) could be achieved at 5 h, which was selected as the suitable reaction time for in-depth studies. Surprisingly, for this specific esterification reaction, one of the reactant (gallic acid) is solid at room temperature, which possess high solubility in the other liquid reactant (n-propanol), meaning that n-propanol is both a reactant and a solvent. Therefore, it is indispensable to investigate the effect of molar ratio of n-propanol to gallic acid on PG conversion, as exhibited in **Figure 4b**. As a result, only 39.5 % yield of PG was achieved at the molar ratio of 2:1, and the PG yield was increased sharply to 93.6 % at the molar ratio of 8:1, but no further improve of PG yield was observed when the molar ratio was increased to 10:1. Thence, the molar ratio of 8:1 for n-propanol and gallic acid was optimal for further study based on the economic benefits. Generally, the catalyst amount has a great effect on the esterification reaction in activity. **Figure 4c** depicts the yield of PG rised evidently from 46.7 % to 95.6 % as the catalyst amount improving from 10 to 40 mg, indicating the best catalyst amount was 40 mg, which represents the best yield of PG than other reported catalysts to our knowledge (**Table S2**).[46-51] Moreover, the cyclical stability of TMeQ[6]-PMA NCs was also evaluated and is displayed in **Figure 4d**. Notably, negligible reduction of the catalytic activity was observed even after recycling for six times, suggesting that the TMeQ[6]-PMA catalysts has excellent stability during esterification reaction. The slight reduce of catalytic activity was ascribed to the no change of crystal structure and morphology without obvious aggregation or agglomeration as supported by XRD pattern and SEM images of TMeQ[6]-PMA NCs (Figure S2 and S3). In addition, the products were further characterized by FTIR and liquid-state ^{1}H magnetic resonance (NMR) spectra, as shown in Figure S4 and S5. The results confirm that product is only PG, no extra by-products are formed, indicating the selectivity of PG is 100%.

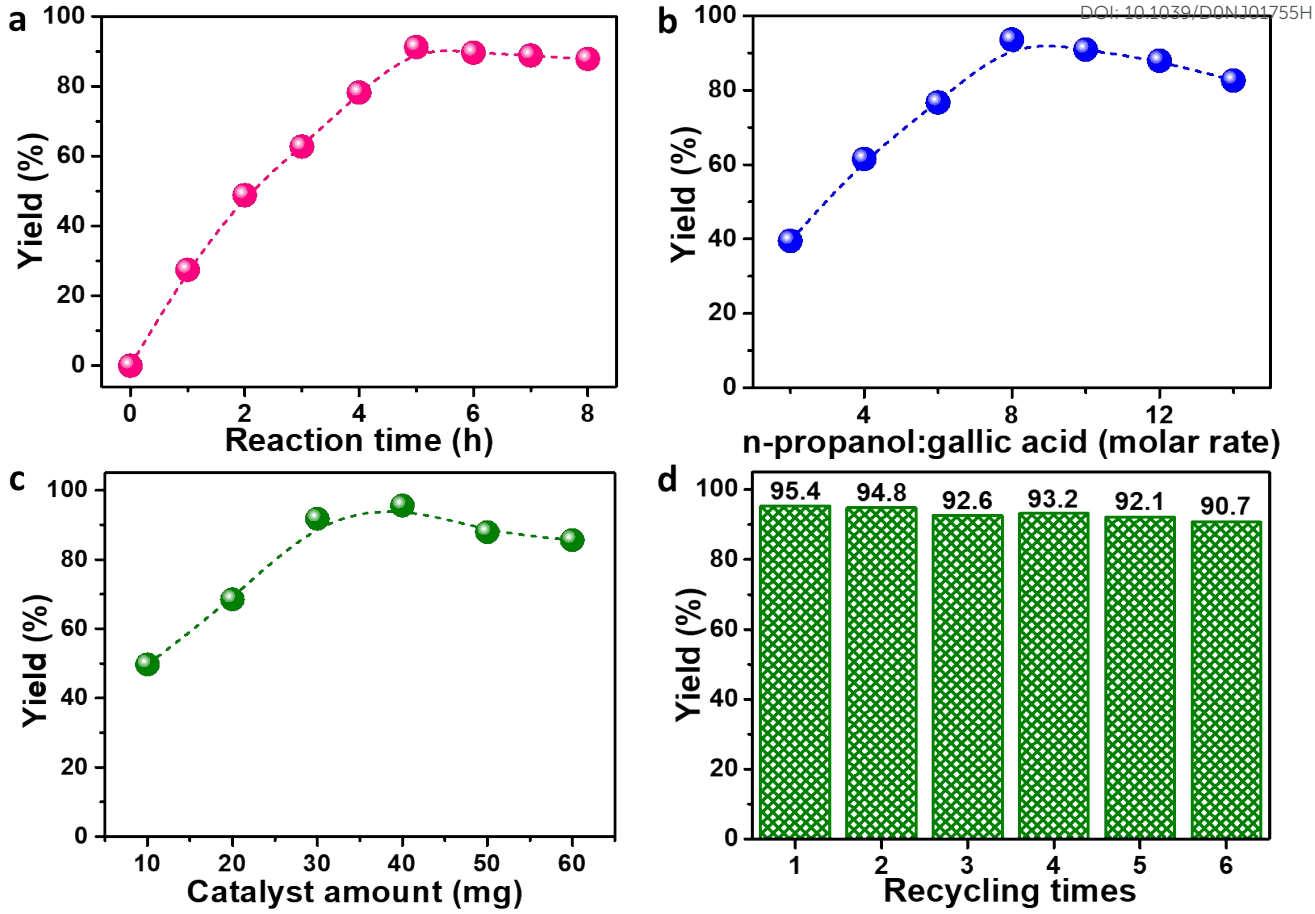

Figure 4. a) Effect of reaction time on the yield of PG. Reaction conditions: catalyst 50 mg, molar rate of reactants 10:1, 80 °C. b) Effect of molar rate of reactants on the yield of PG. Reaction conditions: catalyst 50 mg , 80 °C, 5h. c) Effect of catalyst loading on the yield of PG. Reaction conditions: molar rate of reactants 8:1, 80 °C, 5h. d) Reusability of catalyst. Reaction conditions: catalyst 40 mg , molar rate of reactants 8:1, 80 °C, 5h.

3. Conclusion

In summary, we prepared a novel Q[*n*]-POMs hybrid with same microshape and nanoscale features, tetramethyl cucurbit[6]uril-phosphomolybdic acid (TMeQ[6]-PMA) NCs, through an facile one-step self-assembly method. A combination investigation (FESEM, TEM and EDX) confirms that as-prepared TMeQ[6]-PMA NCs have a microshape and nanoscale features, and the homogeneous dispersion of PMA on the hybrid. FTIR spectroscopy reveal that the self-assembled mechanism of TMeQ[6] and PMA based on outer-surface interactions. NH_3-TPD-MS and py-FTIR results

demonstrate that the coexistence of medium and strong acid sites and a larger number of Lewis acid sites than the Brönsted acidic sites on the catalyst surface. Consequently, the TMeQ[6]-PMA NCs have achieved a high PG conversion (95.6 %) and excellent stability, which represents the best catalytic performances than other reported catalysts.

Conflicts of interest

There are no conflicts to declare.

Acknowledgements

We acknowledge the support of National Natural Science Foundation of China (No. 51663005, 21761007), Science and Technology Plan Project of Guizhou Province (No. 20175788 and 20185781).

4. Experimental Section

Experimental details are provided in the Supporting Information.

5. Notes and references

1 Y. Y. Liang, Y. G. Li, H. L. Wang, J. G. Zhou, J. Wang, T. Regier and H. J. Dai, *Nat. Mater.*, 2011, **10**, 780.

2 J. Y. Lee, O. K. Farha, J. Roberts, K. A. Scheidt, S. B. Ngugen and J. T. Hupp, *Chem. Soc. Rev.*, 2009, **38**, 1450.

3 T. Okuhara, *Chem. Rev*., 2002, **102**, 3641.

4 S. Kobayashi and K. Manabe, *Acc. Chem. Res.*, 2002, **35**, 209.

5 H. Chen, T. Liu, P. Zhou, S. Li, J. Ren, H. He, J. Wang, N. Wang, S. Guo, *Adv. Mater*., 2020, **32**, 1905661.

6 J. Zhang, A. Das, R. S. Assary, L. A. Curtiss and E. Weitz, *Appl. Catal. B. Environ*., 2016, **181**, 874.

7 Q. Y. Liu, H. Y. Wang, H. S. Xin, C. G. Wang, L. Yan, Y. X. Wang, Q. Zhang, X. H. Zhang, Y. Xu, G. W. Huber and L. L. Ma, *Chemsuschem*., 2019, **12**, 3977.

8 H. Chen, Q. Luo, T. Liu, J. Ren, S. Li, M. Tai, H. Lin, H. He, J. Wang, N. Wang, *Small*., 2019, **15**, 1904372.

9 X. Hu, G. K. Chuah and S. Jaenicke, *Appl. Catal. A. General*., 2001, **209**, 117.

10 P. Bhattacharya, E. B. Hassan, P. Steele, J. Cooper and L. Ingram, *BioResources*., 2010, **5**, 908.

11 D. L. Long, R. Tsunashima and L. Cronin, *Angew. Chem. Int. Edit*., 2010, **49**, 1736.

12 H. N. Miras, J. Yan, D. L. Long and L. Cronin, *Chem. Soc. Rev*., 2012, **41**, 7403.

13 M. Bonchio, Z. Syrgiannis, M. Burian, N. Marino, E. Pizzolato, K. Dirian, F. Rigodanza, G. A. Volpato, G. La Ganga, N. Demitri, S. Berardi, H. Amenitsch, D. M. Guldi, S. Caramori, C. A. Bignozzi, A. Sartorel and M. Prato, *Nat. Chem*., 2019, **11**, 146.

14 M. Bosco, S. Rat, N. Dupre, B. Hasenknopf, E. Lacote, M. Malacria, P. Remy, J. Kovensky, S. Thorimbert and A. Wadouachi, *Chemsuschem*., 2010, **3**, 1249.

15 H. Chen, Q. Luo, T. Liu, M. Tai, J. Lin, V. Murugadoss, H. Lin, J. Wang, Z. Guo, N. Wang, *ACS Appl. Mater. Interfaces.*, 2020, **12**, 13941.

16 X. M. Yan, J. H. Lei, D. Liu, Y. C. Wu and L. P. Guo, *J. Chin. Chem. Soc*., 2007, **54**, 911.

17 X. M. Yan, P. Mei, J. H. Lei, Y. Z. Mi, L. Xiong and L. Guo, *J. Mol. Catal. A: Chem.*, 2009, **304**, 52.

18 N. Bhatt, C. Shah and A. Patel, *Catal. Lett*., 2007, **117**, 146.

19 H. Chen, Z. Mu, Y. Li, Z. Xia, Y. Yang, F. Lv, J. Zhou, Y. Chao, J. Wang, N. Wang, S. Guo, *Sci. China. Mater*., 2020, **63**, 483.

20 X. M. Zhang, Z. H. Zhang, B. H. Zhang, X. F. Yang, X. Chang, Z. Zhou, D. H. Wang, M. H. Zhang and X. H. Bu, *Appl. Catal. B. Environ*., 2019, **256**, 117804.

21 H. B. Wu, B. Y. Xia, L. Yu, X. Y. Yu and X. W. D. Lou, *Nat. Commun*. 2015, **6**, 6512.

22 H. IIbeygi, I. Y. Kim, M. G. Kim, W. Cha, P. S. M. Kumar, D. H. Park and A. Vinu, *Angew. Chem. Int. Edit*., 2019, **58**, 10849-10854.

23 J. C. Ye, J. J. Chen, R. M. Yuan, D. R. Deng, M. S. Zheng, L. Cronin and Q. F. Dong, *J. Am. Chem. Soc*., 2018, **140**, 3134.

24 J. Tian, Z. Y. Xu, D. W. Zhang, H. Wang, S. H. Xie, D. W. Xu, Y. H. Ren, H. Wang, Y. Liu and Z. T. Li, *Nat. Commun*., 2016, **7**, 11580.

25 Q. D. Liu, P. L. He, H. D. Yu, L. Gu, B. Ni, D. Wang and X. Wang, *Sci. Adv*., 2019, **5**, 1.

26 L. Isaacs, *Chem. Commun*., 2009, **6**, 619.

27 F. Biedermann, V. D. Uzunova, O. A. Scherman, W. M. Nau and A. De Simone, *J. Am. Chem. Soc*., 2012, **134**, 15318.

28 X. L. Ni, X. Xiao, H. Cong, Q. J. Zhu, S. F. Xue and Z. Tao, *Acc. Chem. Res*., 2014, **47**, 1386.

29 A. I. Lazar, F. Biedermann, K. R. Mustafina, K. I. Assaf, A. Hennig and W. M. Nau, *J. Am. Chem. Soc*., 2016, **138**, 13022.

30 C. F. Li, L. M. Du, W. Y. Wu and A. Z. Sheng, *Talanta*., 2010, **80**, 1939.

31 U. Akiba, D. Minaki and J. Anzai, *Polymers*., 2018, **10**, 130.

32 X. K. Fang, P. Kögerler, L. Isaacs, S. Uchida and N. Mizuno, *J. Am. Chem. Soc*. 2009, **131**, 432-433.

33 M. N. Cao, J. X. Lin, J. Lu, Y. L. J. You, T. F. Liu and R. Cao, *J. Hazard. Mater*., 2011, **186**, 948.

34 J. Lu, J. X. Lin, X. L. Zhao and R. Cao, *Chem. Commun*., 2012, **48**, 669.

35 X. Xia, W. W. Ge, H. Y. Chen, Z. Tao, Y. Q. Zhang, G. Wei and K. Chen, *New J. Chem*., 2019, **43**, 10297.

36 J. Li, D. Li, J. Xie, Y. Liu, Z. Guo, Q. Wang, Y. Lyu, Y. Zhou, J. Wang, *J. Catal*., 2016, **339**, 123.

37 Y. Leng, J. Wang, D. Zhu, X. Ren, H. Ge, L. Shen, *Angew. Chem. Int. Edit*., 2009, **48**, 168.

38 J .E. N. Dolatabadi and S. Kashanian, *Food. Res. Int*., 2010, **43**, 1223.

39 K. T. Chung, T. Y. Wong, C. I. Wei, Y. W. Huang and Y. Lin, *Rev. Food Sci*., 1998, **38**, 421.

40 H. J. Jung and C. J. Lim, *Phytother. Res*., 2011, **25**, 1570.

41 K. S. Sing, *Pure. Appl. Chem*., 1982, **54**, 2201.

42 P. Berteau and B. Delmon, *Catal. Today*., 1989, **5**, 121.

43 J. Y. Luo, K. Kamasamudram, N. Currier and A. Yezerets, *Chem. Eng. Sci*., 2018, **190**, 60.

44 E. P. Parry, *J. Catal*., 1963, **2**, 371.

45 V. M. Benítez, J. C. Yori, C. R. Vera, C. L. Pieck, J. M. Grau, J. M. Parera, *Ind. Eng. Chem. Res*., 2005, **44**, 1716.

46 C. Zhang, X. Y. Pan, M. J. Yu, L. Jing and G. Wu, *Chem. Eng. J*., 2012, **209**, 464.

47 A. Sharma, A. Kumar, K.R. Meena, S. Rana, M. Singh and S.S. Kanwar, *J. King Saud Univ. Sci*. 2017, **29**, 536.

48 F. L. Gloria, M. B. Juan, R. M. Javier, A. C. Jose, M. Rosario, D. L. R. Blanca, V. C. Alfonso and M. G. Jose, *Food. Chem*., 2011, **128**, 214.

49 G. J. Nie, Z. M. Zheng, W. J. Yue, Y. Liu, H. Liu, P. Wang, G. H. Zhao, W. R. Cai and Z. L. Xue, *Process. Biochem*., 2014, **49**, 277.

50 G. J. Nie, H. Liu, Z. Chen, P. Wang, G. H. Zhao and Z. M. Zheng, *J. Mol. Catal. B Enzym*. 2012, **82**, 102.

51 X. W. Yu, Y. Q. Li and S. M. Zhou, *J. Microbiol. Biotechnol*., 2007, **23**, 1091.

View Article Online
DOI: 10.1039/D0NJ01755H

Table of Contents Entry

A novel class of cucurbit[n]urils-polyoxometalates (Q[n]-POMs) hybrids, tetramethyl cucurbit[6]uril-phosphomolybdic acid (TMeQ[6]-PMA) nanocubes (NCs), are synthesized *via* one-step self-assembly method.